Diffraction in low-energy electron scattering from DNA: Bridging gas-phase and solid-state theory

Laurent Caron* and Léon Sanche
Groupe de Recherches en Sciences des Radiations, Faculté de Médecine, Université de Sherbrooke, Sherbrooke, Quebec, Canada QC J1H 5N4

Stefano Tonzani
Department of Chemistry, Northwestern University, Evanston, Illinois 60208-3113, USA

Chris H. Greene
Department of Physics and JILA, University of Colorado, Boulder, Colorado 80309-0440, USA
(Received 27 March 2008; published 27 October 2008)

Using high-quality gas phase electron scattering calculations and multiple scattering theory, we attempt to gain insights into the radiation damage to DNA induced by secondary low-energy electrons in the condensed phase, and to bridge the existing gap with the gas phase theory and experiments. The origin of different resonant features (arising from single molecules or diffraction) is discussed and the calculations are compared to existing experiments in thin films.

DOI: 10.1103/PhysRevA.78.042710 PACS number(s): 34.80.Bm, 87.15.A−, 87.64.Bx

I. INTRODUCTION

Since the discovery [1] that low-energy electrons (LEE) can cause strand breaks in the DNA duplex, the interest in electron interactions with DNA, which originates primarily from its importance in radiation damage to living tissue and radiotherapy, has grown consistently [2]. The impact of ionizing electromagnetic radiation on matter causes the emission of highly energetic electrons; these latter ionize the medium via an electromagnetic type of interaction, thus producing secondary electrons in large numbers [3]. Most secondary electrons are created with low energy ($E < 20$ eV) and have a distribution with a most probable energy of 9 eV [4]. If the electron energy is above the DNA ionization threshold (7–10 eV) these electrons can ionize it, while over the entire 0–15 eV range they can be captured in a resonant anionic state. Fast, efficient dissociation pathways are known to exist for organic molecules [5] from electronic dissociative states, dissociative electron attachment, dipolar dissociation, and dissociative ionization, which can be related to capture or transfer of an electron or hole into a dissociative state [6,7].

In the context of subionization threshold electrons, the importance of resonances has become evident. Specifically, electron capture by a DNA subunit to form a molecular resonance enhances greatly the rupture of chemical bonds within the molecule either by dissociative electron attachment (DEA) or the decay of the transient anion into a dissociative electronically excited state. These phenomena are reflected in the measured yield of strand breaks which exhibit prominent resonant features as a function of energy [8].

In a condensed environment, LEE are created within or outside DNA. The former necessarily have a high probability to interact with DNA. LEE created outside DNA may also interact with this molecule depending on the time scale of thermalization of the electrons. In this case, other types of damage, such as radical-mediated damage, can become important or even predominant. In general, if the thermalization is slow, DNA is impacted by a relatively hot electron (meaning in this context an electron not fully solvated) from outside; this entails usually a time scale between 0.1 and 100 fs [9]. Others created outside the DNA do not arrive at the target with any appreciable energy and therefore cannot directly damage it, but they can form radicals along the way, and these in turn can attack the DNA [10]. The prevalence of one or the other of these mechanisms is probably determined by the DNA concentration: if it is high, then the electrons are more likely to be created within DNA or impact it before being completely solvated. In principle, modeling the dynamics of the radiation tracks [11] can yield very useful information in this regard.

Since radiation damage in a cell is a complicated problem, researchers have tried to simplify its description by observing first what happens to DNA components in the gas phase when impacted by LEEs; this literature is by now rather vast. The experimental approaches have been focused mostly on predicting products of dissociative electron attachment from DNA subunits and determining the role of shape resonances [12–15]. The theoretical community has provided information on resonances in elastic and inelastic scattering [16–20]. While dissociative electron attachment calculations for these large targets are still beyond reach, quantum chemical methods have been employed to predict the weakest bonds in electron attachment [6,21] and study the hydration effects on the anionic compounds [22]. It must be noted, however, how none of these methods will be able for the foreseeable future to deal with a molecule of tens of thousands of atoms like bacterial DNA in a process in which both electronic and

*Permanent address: Département de Physique et Regroupement québécois sur les Matériaux de Pointe, Université de Sherbrooke, Sherbrooke, Quebec, Canada QC J1H 5N4.
Electronic address: laurent-g.caron@usherbrooke.ca

nuclear degrees of freedom are involved, the scattering electron is unbound, and the solvent has to be considered as well. While density functional theory (DFT) is able to deal with large systems, nuclear dynamics on DFT surfaces is not as well defined [23,24] and a scattering theory using DFT is just starting to be developed [25].

This work aims to be a first step toward systematizing what happens in passing from the gas to the condensed phase. In particular, we will be concerned with the solid state, since this gives us the opportunity to relate to radiation damage experiments in thin film [1,2] and, equally importantly, to neglect fluctuations in the DNA structure, which are of fundamental importance in solution [26,27].

To this extent, the first step is to understand what happens inside the DNA polymer itself, which is represented here as rigid and immersed in vacuum. In this context, it is possible to explore parameters like DNA sequence and conformation, which could be important in radiobiological damage.

We pursue this goal using a model, described below, which unites a recently developed multiple scattering framework [28–31] with accurate electron scattering calculations for the DNA bases performed using the *R*-matrix method [16,32]. This proposed model differs from the one recently utilized by Orlando *et al.* [33] in that their multiple scattering approach is on the individual atoms comprising all of the subunits and is only to first order in the scattering. We believe that our more rigorous framework will eventually provide a better description of physical systems, even though we only include the DNA bases in the present calculation.

In our model, we have left out of the picture, for the moment, all the properties of the liquid phase, from fluctuations to the motion of the solvated electron in water. We plan to introduce the structural water (also present in thin films) as a scattering dopant and the backbone in further studies using this model, which will be fairly straightforward. To introduce the liquid phase properties [34] instead would be much more difficult and require some essential modification to this framework.

II. MODEL

The multiple scattering (MS) framework we shall be using to get information on the elastic scattering of low-energy electrons (LEE) has been described in the series of articles by Caron and Sanche [28–31]. It was developed at a time when no scattering matrix information was available for the DNA bases. The objective of the toy model used was to find trends in cross sections and capture amplitudes resulting from regularity or disorder in the helix and base sequencing. With the advent of recently available scattering information on DNA bases, it is important to revisit elastic LEE scattering on DNA to get more precise numerical estimates and ascertain whether the previous conclusions are still valid. One obvious difference of the current calculations with respect to Refs. [28–31] is the presence of shape resonances that carry over from the gas phase scattering of the subunits, which makes it possible to observe the fate of local resonances in the conjugate. We shall first study, in this paper, the idealized B-form of a GCGAATTGGC decamer (without backbone) [35] and its regularly sequenced cousin, the poly(A)·poly(T) base pairs decamer. We shall then examine the A-form of the GCGAATTGGC decamer [35]. These structures are chosen to be ideal ones, although they are in general known to be slightly different [36]. Both forms of DNA are sufficiently different to warrant a separate examination: the B-form of DNA has 10 base pairs per helical turn (thus our choice of a decamer) and hence a 36.0 degree helical twist, a small tilt (2.8 degree inclination) relative to the spiral axis but appreciable roll (−15.1 degrees propeller twist) of the base pairs, a rise of 0.338 nm between successive base pairs; the A-form has 11 base pairs per helical turn and hence a 32.7 degree helical twist, has considerable more tilt (22.6 degree inclination) and slightly less roll (−10.5 degrees propeller twist) of the base pairs, and has a much smaller rise of 0.254 nm [37].

But let us first review the theoretical framework. Note that all equations will be expressed in atomic units (a.u.) in which the bohr radius is the unit of length and the hartree (2 Ry) is the unit of energy.

A. Multiple scattering theory

In Refs. [28,29], we presented the basic equations for multiple electron scattering within macromolecules, including DNA. For the latter, we proposed a simple model of molecular subunits (i.e., bases, sugars, and phosphates) immersed in an optical potential U_{op}, which is constant between their *R*-matrix shells (or between the muffin tins), a working hypothesis that has been used in the calculations for simple molecules [38] in the theory of low-energy electron diffraction (LEED) in solids [39] and nanoscale structures [40]. The only function of the real part of the optical potential is to account for the average energy seen by an electron. One can quite generally describe the scattering problem of a molecular subunit by its scattering matrix $S_{L'L}$ [41,42], where $L=(l,m)$ are the angular momentum quantum numbers. Each molecular subunit has an incident plane wave of momentum $\vec{k}$ impinging on it plus the scattered waves of all other subunits. More specifically, we described the asymptotic form of the total wave function $\psi_{\vec{k}}^{(n)}(\vec{r})$ for a molecule centered at $\vec{R}_n$ outside the *R*-matrix shell by the following equation:

$$\psi_{\vec{k}}^{(n)}(\vec{r}) = 4\pi e^{i\vec{k}\cdot\vec{R}_n} \sum_{LL'} i^l B_{\vec{k}L}^{(n)} Y_{L'}(\Omega_{\vec{r}_n}) \left[j_l(kr_n)\delta_{L'L} + \frac{1}{2}(S_{L'L}^{(n)} - \delta_{L'L}) h_{l'}^{(1)}(kr_n) \right], \tag{1}$$

where Y_L are spherical harmonics, j_l and $h_{l'}^{(1)}$ are the spherical Bessel function and Hankel function of the first kind, respectively, $\vec{r}_n = \vec{r} - \vec{R}_n$, and

$$B_{\vec{k}L}^{(n)} = Y_L^*(\Omega_{\vec{k}}) + \frac{1}{2} \sum_{n' \neq n} \sum_{L_1,L_2,L_2'} i^{l_1+l_2-l_2'} B_{\vec{k}L_2}^{(n')} (S_{L_2'L_2}^{(n')} - \delta_{L_2'L_2}) \times (-1)^{m_2'} e^{-i\vec{k}\cdot\vec{R}_{nn'}} F_{m_1,m,-m_2'}^{l_1,l,l_2'} Y_{L_1}(\Omega_{\vec{R}_{nn'}}) h_{l_1}^{(1)}(kR_{nn'}), \tag{2}$$

where

$$F^{l_1,l,l_2'}_{m_1,m,-m_2'} = [4\pi(2l_1+1)(2l+1)(2l_2'+1)]^{1/2} \times \begin{pmatrix} l_1 & l & l_2' \\ 0 & 0 & 0 \end{pmatrix} \begin{pmatrix} l_1 & l & l_2 \\ m_2' & m & -m_2' \end{pmatrix},$$

and $\begin{pmatrix} l_1 & l & l_2' \\ m_1 & m & -m_2' \end{pmatrix}$ is the Wigner 3-j symbol, [43] and $\vec{R}_{nn'} = \vec{R}_n - \vec{R}_{n'}$. Equation (2) implies a coupled set of linear equations for all $B^{(n)}_{\vec{k}L}$, which measure the resultant of the superposition of the incident plane wave and the contribution from all other scatterers. As mentioned before [28,29], the loss of coherence of the electrons due to inelastic collisions can be invoked through an imaginary part in the background optical potential U_{op} [39], i.e., an imaginary part to the electron wave number $\text{Im}(k) = \xi^{-1}$. Here ξ acts as a coherence length for the electrons. In this paper, we have set the coherence length to a value much larger than the decamer dimensions (1000 a.u.) so as to reproduce a negligible loss situation.

B. Electron capture and scattering

In an effort to extract physically meaningful information from the multiple scattering formalism, we had previously targeted a calculation of the capture amplitude $V^{(n)}_{\vec{k}}$ of an electron in a shape or core excited resonance of a basic subunit positioned at $\vec{R}_n$. We had assumed a dominant capture channel symmetry corresponding to L_o and had used the one-center approximation of O'Malley and Taylor [44]. When generalized to a multiple scattering situation, this leads to

$$V^{(n)}_{\vec{k}} = \sqrt{4\pi} V_{l_o} B^{(n)}_{\vec{k}l_o} e^{i\vec{k}\cdot\vec{R}_n}, \tag{3}$$

where V_{l_o} is an energy and nuclear coordinate-dependent amplitude. This amplitude contains the dissociative attachment information. There is unfortunately no available theoretical information on the nuclear part of the wave function for the DNA bases at this time. So we shall only focus on the MS part $B^{(n)}_{\vec{k}l_o}$.

We proposed [30] a weighted partial capture factor

$$\Gamma_w(l_o) = \frac{\Sigma_{\vec{R}_n} \gamma(l_o, \vec{R}_n)}{\Sigma_{\vec{R}_n}}, \tag{4}$$

in which the constituent partial capture factor

$$\gamma(l_o, \vec{R}_n) = \frac{\Sigma^{l}_{m_o=-l} |\sqrt{4\pi} B^{(n)}_{\vec{k}l_o m_o}|^2}{(2l+1)} \tag{5}$$

measures the partial wave decomposition of the total wave function at $\vec{R}_n$. Any dissociative attachment resonance occurring in the l_o channel would lead to a capture probability that, by Eq. (3), is modulated by $|B^{(n)}_{\vec{k}l_o}|^2$. $\gamma(l_o, \vec{R}_n)$ can serve as a meaningful measure of the effect of MS on dissociative attachment. Since $\gamma(l_o, \vec{R}_n) = 1$ for a lone plane wave, then any value larger than 1 would imply an enhancement of the dissociative attachment resonance cross section due to MS. Note that $\gamma(0, \vec{R}_n)$ equals the absolute square of the wave function at $\vec{R}_n$, and $\Gamma_w(0)$ measures the absolute square of the wave function averaged over all bases.

The total elastic cross section, for a finite-size macromolecule, is also of interest. Technically, we can expand the scattered part of Eq. (1) around the geometric center $\vec{R}_{\text{GC}}$ of the macromolecule. In this reference system, remembering that $\vec{r}_n = \vec{r} - \vec{R}_n$, one has

$$Y_{L'}(\Omega_{\vec{r}_n}) h^{(1)}_{l'}(kr_n) = \sum_{L_1,L_2} i^{l_1+l_2-l'} (-1)^{m'} F^{l_1,l_2,l'}_{m_1,m_2,-m'} Y_{L_1}(\Omega_{\vec{r}-\vec{R}_{\text{GC}}}) \times Y_{L_2}(\Omega_{\vec{R}_{\text{GC}}-\vec{R}_n}) h^{(1)}_{l_1}(k|\vec{r}-\vec{R}_{\text{GC}}|) j_{l_2} \times (k|\vec{R}_{\text{GC}} - \vec{R}_n|). \tag{6}$$

In the limit $k|\vec{r}-\vec{R}_{\text{GC}}|$ large, one can write

$$\lim_{k\rho \text{ large}} h^{(1)}_{l_1}(k\rho) = i^{-l_1-1} e^{ik\rho}/(k\rho), \tag{7}$$

where $\vec{\rho} = \vec{r} - \vec{R}_{\text{GC}}$. Therefore, one obtains

$$\lim_{k\rho \text{ large}} \psi^{(n)}_{\vec{k}}(\vec{\rho}) = 2\pi \sum_{LL'} e^{i\vec{k}\cdot\vec{R}_n} i^l B^{(n)}_{\vec{k}L} T^{(n)}_{L'L} \sum_{L_1,L_2} i^{l_1+l_2-l'} (-1)^{m'} \times F^{l_1,l_2,l'}_{m_1,m_2,-m'} Y_{L_1}(\Omega_{\vec{\rho}}) \times Y_{L_2}(\Omega_{\vec{R}_{\text{GC}}-\vec{R}_n}) j_{l_2} \times (k|\vec{R}_{\text{GC}} - \vec{R}_n|) i^{-l_1-1} e^{ik\rho}/(k\rho), \tag{8}$$

where

$$T^{(n)}_{L'L} = [S^{(n)}_{L'L} - \delta_{L'L}] \tag{9}$$

is the T-matrix. From this, one can calculate the scattered current at distance ρ divided by the incident electron flux. In doing this, one obtains the following definition for the elastic cross section in the lossless situation:

$$\sigma_e(k) = \sum_{L_1} |\phi_{L_1}|^2/|k|^2, \tag{10}$$

$$\phi_{L_1} = 2\pi \sum_{nLL'} e^{i\vec{k}\cdot\vec{R}_n} B^{(n)}_{\vec{k}L} T^{(n)}_{L'L} \sum_{L_2} i^{l+l_2-l'-1} (-1)^{m'} F^{l_1,l_2,l'}_{m_1,m_2,-m'} \times Y_{L_2}(\Omega_{\vec{R}_{\text{GC}}-\vec{R}_n}) j_{l_2}(k|\vec{R}_{\text{GC}} - \vec{R}_n|). \tag{11}$$

C. *R*-matrix calculations

The static-exchange approximation [45] reduces the problem of electron scattering from a polyatomic molecule to a one-electron problem; our model contains also a local correlation-polarization potential. The static exchange approximation amounts to including only the ground state of the target in the close-coupling expansion of the wave function, and it is roughly the equivalent of the Hartree-Fock approximation for continuum states [46]. A detailed description of our method can be found in Refs. [16,32,47,48]; here we just sketch the main points of the treatment.

We use the *R*-matrix method to solve the one-electron problem [16]. This method consists of partitioning space into a short-range zone, where all the channels are coupled and

the scattering problem can in principle be treated in all its many-body complexity, and an outer zone (external to the target electron density) in which the escaping electron only sees the effect of the target molecule as a multipole expansion of the electrostatic potential. In passing, we note that this is conceptually very suitable to the scheme we are applying in this work, patching together short-range scattering data for various DNA subunits, and it also allows us to get rid of the long-range (dipole) part of the electron molecule interactions, which is not relevant here. In its eigenchannel form, the *R*-matrix method can be formulated as a variational principle [49] for the normal logarithmic derivative $(-b)$ of the wave function on the reaction zone surface,

$$b \equiv -\frac{\partial \log(r\Psi)}{\partial r} = 2\frac{\int_V \Psi^*(E-\hat{H}-\hat{L})\Psi dV}{\int_V \Psi^* \delta(r-r_0)\Psi dV}, \qquad (12)$$

where $\hat{L}$ is the Bloch operator, needed to make the Hamiltonian $\hat{H}$ Hermitian, and r_o is the boundary between the internal and external regions. It is possible, after expanding the internal region wave function in a suitable basis set, to recast the solution of Eq. (12) as an eigenvalue problem and then through basis-set partitioning to shift the computational burden to the solution of a large linear system [16,49]. As a basis set, we use finite elements [50] in all three spherical coordinates; in this way, we have large but sparse matrices that are amenable for solution with fast sparse solvers [47,51].

A further simplification consists in using the local density approximation (LDA) for the exchange potential,

$$V_{\text{ex}}(\vec{r}) = -\frac{2}{\pi}k_F F(k_F,E), \qquad (13)$$

where k_F is the local Fermi momentum,

$$k_F(\vec{r}) = [3\pi^2\rho(\vec{r})]^{1/3}, \qquad (14)$$

F is a functional of the energy and the local density $\rho(\vec{r})$ (through the local Fermi momentum), and $\vec{r}$ is defined relative to the center of mass of the molecular fragment being considered. The functional form we use for F is called the Hara exchange [52]. It has been extensively employed in continuum state calculations, and it is energy-dependent. The LDA, widely used also in DFT calculations [53], gives qualitatively correct results [16,45], while it is simple enough to allow calculations for complex molecular targets.

A polarization-correlation potential is added to this. The long-range part of this potential is a simple multipole expansion, of which we retain only the induced dipole polarization term,

$$V_{\text{pol}} = -\frac{\alpha_0}{2r^4}, \qquad (15)$$

where α_0 is the totally symmetric component of the polarizability tensor (higher-order and anisotropic terms are much less important [48]), and it can be calculated *ab initio* using electronic structure codes. This potential is in principle nonlocal inside the target molecule. We approximate it as a local potential using a form based on DFT [specifically on the Lee-Yang-Parr (LYP) potential of Ref. [54]], which has yielded reliable results in the work of Gianturco and coworkers. [55] This form makes use of the electron density, its gradient, and Laplacian, which have to be calculated for each target molecule. The short- and long-range potentials are matched unambiguously (continuously but with discontinuous derivatives) at the innermost crossing point, whose radius is dependent on the angles. The matching is unambiguous in the sense that there are two crossing points between the inner and outer potential for each angle, and we always choose the innermost, since the other is far in the region where the electron density of the molecule is very small. Choosing the outermost crossing has proven to give unphysical results [56] in many cases.

All the target quantities are calculated at the Hartree-Fock level using a 6-31G** basis set, and the target equilibrium geometries have been optimized at the same level of theory. The details of the calculations have been described in Ref. [16], including the convergence criteria. We notice here that the cross sections for the purines had to be recalculated due to an error in the calculation of the electron density, as noted in Refs. [48,57], and their resonances are now shifted to lower energy with respect to Ref. [16]. These calculations are very cumbersome, and for the level of accuracy we are aiming for here, this convergence criterion seems adequate.

III. RESULTS AND DISCUSSION

A. B-form poly(A)·poly(T) base pairs decamer

We found it judicious to start our study with the very regular poly(A)·poly(T) decamer (with one strand containing 10 adenines and the other 10 thymines, not considering the backbone) in order to avoid sequence disorder and focus more on the regularity of the spiral structure. This should favor comparisons with the previous toy model simulations, which predicted important effects of internal diffraction and enhancement of capture amplitudes at low energy [28,29]. It will also allow us to make contact with the nontriviality of combining *R*-matrix calculations with MS theory for dipolar molecules. The ground rules for a satisfactory integration were laid in the recent studies of the H_2O molecule in solid ice [58] and the water dimer [59].

The work on solid ice [58] has shown that a cutoff in the range of action of the dipole must be introduced. Without one, no physically meaningful electron energy band structure can be obtained for ice at low energy. One might think that it should be cut off at the radius of the contact spheres R_c (half the near-neighbor distance), as is normally the case for a centro-symmetric atom [60,61]. But this is far from obvious since the dipole energy $E_{\text{dip}}=-\vec{d}\cdot\hat{r}/r^2$ is angle-dependent and there can be no matching of the potential energy of the scatterer with the flat U_{op} of our MS theory between *R*-matrix spheres [60,61]. Removing the dipole field for $r>a_c$, where a_c is a cutoff radius equal to the *R*-matrix sphere size in our case, is also done at the cost of introducing an anisotropic discontinuity $-2\vec{d}\cdot\hat{r}/a_c^2$ at the edge $r=a_c$. As a_c decreases, more dipole is removed but the discontinuity increases. There is hopefully a tradeoff at some intermediate value of a_c

at which the scattering reasonably represents that of the core of the molecule while minimizing the mismatch. Admittedly, this is an ad hoc procedure. By varying the R-matrix sphere radius, one could tune the T-matrices to best fit available data, as done in [58]. It was found in [58] as well as by a number of authors (see [62]) that this radius is not critical and seems to work best, in ice and the water dimer, when it is slightly larger than the intermolecular distance. There is also the need of a cutoff on the angular momentum components of the T-matrix. We shall come back to this second cutoff shortly.

We used the atomic coordinates of an AT pair in the idealized structure data file obtained from the Protein Explorer Internet site [35] and generated the decamer by rotating this structure by 36 degrees and translating it by 3.38 Å along the spiral axis [37]. Our S matrices were calculated using a dipole cutoff at 11 a.u., the size of our R-matrix box. The reasoning behind this is that the superposition of the long-range part of the polarization potential coming from all bases would nearly cancel out and, in any case, be absorbed into the optical potential. The S matrices of adenine and thymine had to be rotated so that their principal molecular axes coincided with those of the corresponding bases in the decamer. Three orthogonal axes were defined for each base from the positions of the C2, C4, and C6 atoms of the ring part [37], $\vec{a}_{Ri}$ for the R-matrix molecule positioning and $\vec{a}_{dj}$ for the decamer base orientation $(i,j=1,2,3)$. The following transformation is inspired by Messiah's [43] treatment of rotations. We define three Euler angles α, β, and γ from the following association of

$$R(\alpha,\beta,\gamma)_{i,j} = \vec{a}_{Ri} \cdot \vec{a}_{dj} \tag{16}$$

with Eq. (C.45) of Messiah. The transformation matrix is then defined as

$$W_{lm,lm'} = e^{-i\alpha m} \tau^{(l)}_{mm'}(\beta) e^{-i\gamma m'}, \tag{17}$$

where $\tau^{(l)}_{mm'}(\beta)$ is the y axis rotation matrix defined in Eq. (C.72) of Messiah. The transformed S matrix $\tilde{S}_{lm,l'm'}$ becomes

$$\tilde{S} = WSW^{-1}. \tag{18}$$

Let us now naively use these rotated S matrices in Eq. (2) using the full extent of angular momenta $l \leqslant 8$ obtained in the R-matrix calculations for an incident plane wave having a wave vector $\vec{k}$ perpendicular to the midsection base-pair direction and the spiral axis. Figure 1 shows the total elastic cross section as a function of energy. All calculations were done at 50 energy values in the range 0–13.6 eV. Our energy resolution is thus 0.272 eV. One immediately notices the surprisingly large and suspicious values at the lower energies. The two dominant peaks correspond to some 15 times the geometrical cross section of the decamer. This is not a low-energy dipolar effect as all dipoles are cut off at 11 a.u. in our calculations. As we will see later on, the situation is even more extreme for the other decamer.

The reason for this low-energy unruly behavior of multiple scattering theory using R-matrix results for the scatterers emerged as the study of the H_2O molecule in solid ice

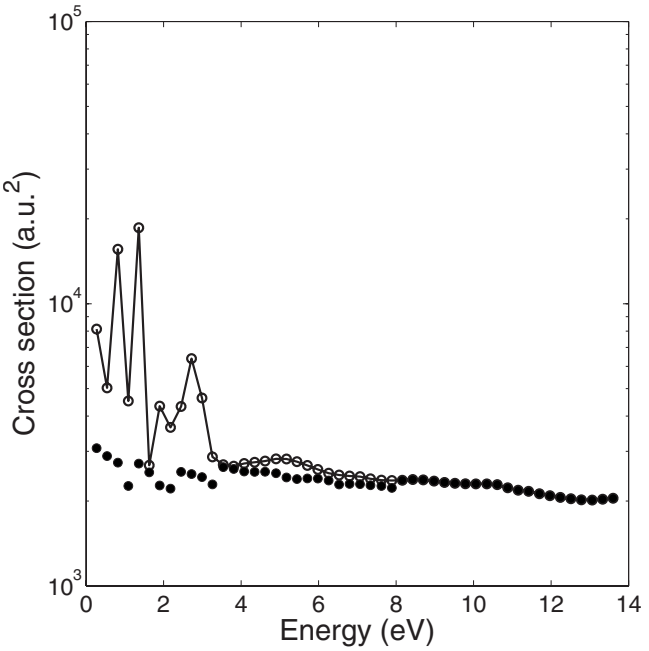

FIG. 1. Total elastic cross section of the poly(A)·poly(T) decamer as a function of incident electron energy using the full angular momentum content of the scattering matrix (full line) or imposing a strict application of the angular momentum cutoff criterion (dark circles).

[58]. In ice, the correct band structure can only be obtained at low energy by cutting off the angular momenta components of the T-matrix to $l \leqslant 2$ instead of using the full range $l \leqslant 4$. The same strategy emerges in the study of the water dimer [59] in which the R-matrix elastic cross section of the dimer can only be correctly reproduced by multiple scattering theory when using this truncation. The need for a cutoff can be understood by the following semiclassical argument. For an electron with angular momentum $L \sim kr$, one can write $L^2 \approx l(l+1) = k^2 r^2$. If $r \gtrsim d_m$, where d_m is the intermolecular distance, then obviously the electron is outside of the interaction space of the two molecules. This means that the relevant angular momenta are those for which $r \lesssim d_m$, i.e.,

$$l(l+1)/k^2 = l(l+1)/(2E_e) \lesssim d_m^2, \tag{19}$$

where E_e is the electron energy. But what is the mathematical reason? Let us look closer at Eq. (2). It turns out that the spherical Hankel function of the first kind $h^{(1)}_{l_1}(kR_{nn'})$, where $R_{nn'}$ is the distance between the two scatterers n and n', diverges as $(kR_{nn'})^{-(l_1+1)}$ for small values of the argument $(kR_{nn'})$. The singularity is dominated by the nearest-neighbor distance d_m. For $l, l'_2 = 4$, l_1 can be as large as $2l = 8$. The reason for this comes from the angular momentum composition rule that says the sum over l_1 can reach the uppermost value of $l_1 \leqslant |l + l'_2|$. So even though the $l'_2 = 4$ components of the T-matrix $T = S - 1$ get smaller as the energy decreases, the product of $h^{(1)}_{l_1}(kR_{nn'})$ with T gets overly large because of the much more singular behavior of the Hankel function. The situation gets much more acute in our case since for $l \leqslant 8$ the sum over l_1 goes up to $l_1 = 16$. This is a consequence of the

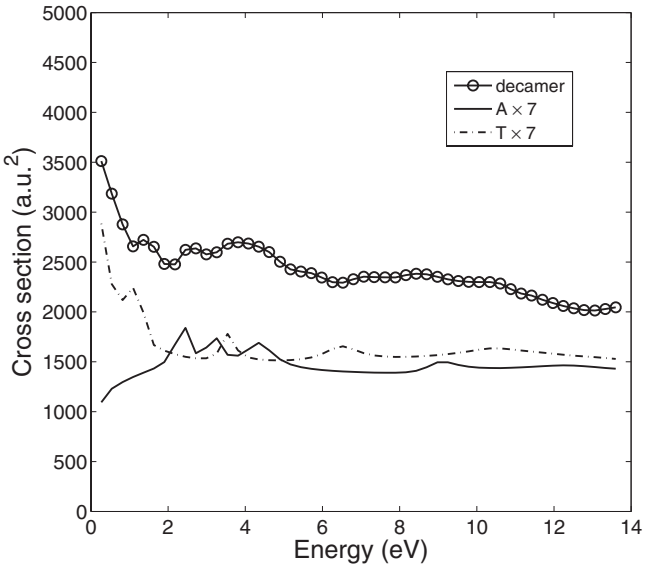

FIG. 2. Interpolated total elastic cross section of the poly(A)·poly(T) decamer compared with the single adenine and thymine *R*-matrix cross-section values as a function of incident electron energy.

close packing of the molecules. Truncating the angular momentum expansion is an inexpensive way of getting rid of this improper behavior.

Our studies on dipolar molecules have shown that this truncation procedure is required for molecules with long-range interactions. This is so regardless of the *R*-matrix radius, even for the value corresponding to the usual muffin-tin radius R_m, which is half the interatomic or intermolecular distance d_m. Neutral atoms and nondipolar molecules, however, have a finite potential cutoff equal to R_m. This means that these scatterers have a T-matrix that has a natural angular momentum cutoff such that $l(l+1)/k^2=l(l+1)/(2E_e) \lesssim R_m^2=d_m^2/4$. It is quite obvious from this that the cutoff condition of Eq. (19) is always satisfied. It is irrelevant in such situations as it is superseded by the natural one. That is why our proposed cutoff procedure is not needed in conventional muffin-type scattering as in Refs. [38,39].

One needs to use a cutoff condition to describe multiple collisions in the decamer. Only values $l \leqslant l_o$ should be retained such that $E(l_o,d_m)<E_e<E(l_o+1,d_m)$, where $E(l_o,d_m)=l(l+1)/(2d_m^2)$. One might think that d_m should be equal to the base stacking distance ≈ 7.3 a.u. along the spiral axis direction. Were one to use this value, then the use of Eq. (19) would wipe out the $L=2,3$ shape resonances [32] of all bases for energies below 3 eV. The lower energy threshold at which the cutoff condition is satisfied for the angular momenta of these shape resonances is larger than the resonance energies. The use of this value of d_m would also distort the elastic cross section of the decamer for energies less than 5 eV. There would be poor correspondence between the signature peaks of the bases and the decamer cross section contrary to the findings of the forthcoming calculations (see Figs. 2 and 6, in which a more realistic value of d_m was used). It is clear that an electron that scatters from one molecule to another does so from every part of the first molecular subunit to every part of the other, including from one end of the one molecule to the diagonally opposite end of the other one. We have thus chosen the value $d_m=11$ a.u., which is of the order of this distance, the size of the bases, the distance between base centers in the base pairs, and the size of the *R*-matrix sphere so as to retain all of its important energy-dependent characteristics. Since the *R*-matrix box and the distance between the base centers have similar values, the multiple scattering spheres overlap with a value similar to that used in ice and the water dimer [58,59]. Overlapping spheres have been used in the past in various other calculations, [62,63] and they are unavoidable in the present case since the bases are large and flat.

But this now poses a new problem having to do with the discreteness of l. A strict imposition of these cutoffs would result in a piecewise chopped cross section, as can be seen in Fig. 1. One way to circumvent this difficulty, which we have adopted throughout, is to interpolate any scalar quantity, calculated for all integer values of angular momenta, at the noninteger value of l obtained from the solution of $E_e=l(l+1)/(2d_m^2)$. A similar procedure was used in a study of a H_2O dimer [59] and the resulting elastic cross section was found to compare very well with the one calculated using the full *R* matrix on the dimer. The result of this procedure on the decamer is shown in Fig. 2. A comparison with the bare molecular cross sections obtained from the *R*-matrix calculation shows good concordance of most of the peaks, with the exception of the one at 6.5 eV in thymine, which is lessened and perhaps split. It should also be mentioned that were the cutoff interpolation procedure used on the calculation of the elastic cross section of the monomers A and T, there would be no visible difference with the results of Fig. 2. This is somewhat reassuring for the credibility of the interpolation procedure.

Let us now look for signs of internal diffraction. As discussed in Refs. [28,29], this would occur because of the regular spacing of base pairs along the spiral axis. We have calculated various quantities that were previously shown to be sensitive to this regular spacing. Figure 3(a) shows the quantity $\Gamma_w(0)$, equal to the average of the square of the electron wave function on the bases. It is compared to the one obtained by dilating the distances along the spiral axis by a factor 1.05. One expects a down shift in energy for those peaks sensitive to the inter-base-pair spacing $d_\parallel$ by some 10% ($E \propto k^2 \propto \lambda^{-2} \propto d_\parallel^{-2}$). Three peaks seem to behave this way, although the one at 11.4 eV at regular spacing is more probably the internal diffraction one that was deduced in the previous publications. The unshifted peak slightly below 2.7 eV is of local origin. Figure 4 shows a contour plot of $\gamma(0,\vec{R}_n)$, the absolute square of the wave function at each base's center, in energy and base sequence space. One must of course realize that these contour lines are calculated by interpolating $\gamma(0,\vec{R}_n)$, which is defined only for a discrete set of the index n. The virtue of such a graph is to enable a quick survey of cool or hot spots at which the square of the wave function is small or large. The sequencing index varies from 1 to 10 going up the A strand and from 11 to 20 going down the T strand. The peak structures in $\Gamma_w(0)$ showing appreciable enhancement of the wave function are seen to occur

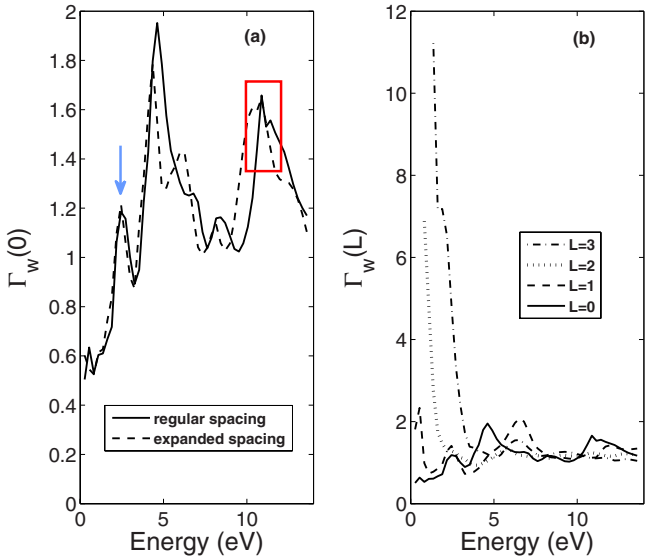

FIG. 3. (Color online) Interpolated values of the weighted partial capture factors for the poly(A)·poly(T) decamer as a function of incident electron energy: (a) $L=0$ component for normal spacing and for an expanded spacing 1.05 times the regular one; (b) $L\leqslant 3$ for normal spacing. The arrow and rectangular area highlight the peak structures at 2.7 and 11.4 eV discussed in the text.

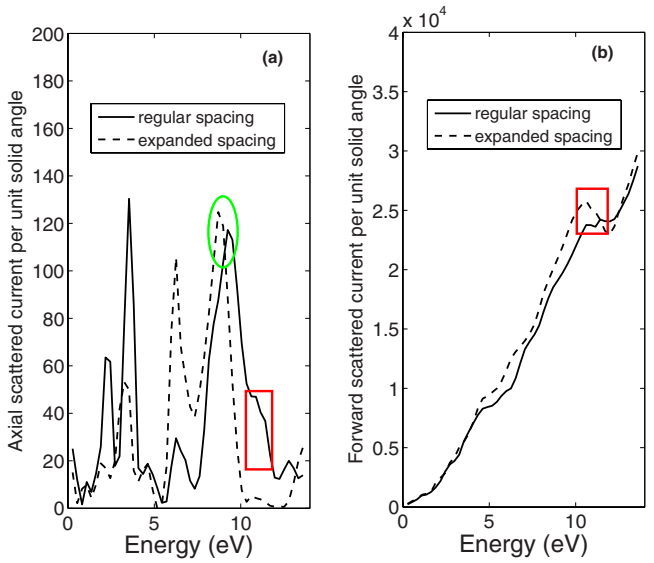

FIG. 5. (Color online) Scattered current in a.u. for the poly(A)·poly(T) decamer as a function of incident electron energy for normal spacing and with an expanded spacing 1.05 times the regular one: (a) in the $+\hat{z}$ direction; (b) in the forward direction. The circled and rectangular areas highlight the peak structures at 9.2 and 11.4 eV discussed in the text.

mostly on the base pairs that lie nearly perpendicular to the incident electron direction (actually, the closest to perpendicular is at an angle of 90 ± 18 degrees), at the beginning ($n=1,20$), middle ($n=5,6,15,16$), and end of the decamer ($n=10,11$), where phase coherence is more favorable. We have also calculated the axially scattered current per unit solid angle in the $+\hat{z}$ direction in Fig. 5(a) and the forward scattered current per unit solid angle in Fig. 5(b) under identical axial spacing conditions as in Fig. 3(a). The only shifting peak that is common to all figures is the one at 11.4 eV at regular spacing. This is clearly the internal diffraction peak. One should note the large peak at 9.2 eV in Fig. 5(a), which dominates over the shouldering 11.4 eV peak. There is nothing special that can be seen in the wave function in Fig. 4 at that energy. This result can only be understood by interference between the scattered beams emanating from the bases. For the current along the axis, aside from the contribution of the beam amplitudes at each base $\vec{R}_n$, there is an extra exit phase factor at position $z\rightarrow\infty$ on the axis outside the decamer, which is proportional to $\exp[ik(z-z_n)]$. This means that there is an optimal value of k at which $\exp[ik(z_{n'}-z_n)]$ between neighboring base pairs along the spiral axis will "synchronize" the beams and produce an overall good phase coherence. The position of the peak yields $k\sim 0.825$ and a $\lambda\sim 7.6$. The vertical distance between base pairs is 6.4 a.u.. Why do the numbers not match? This is because we are dealing with a complex superposition of many different partial waves with different phases for all l (and m) less than or equal to 8. The optimal value of λ has to compromise with all of these, and this happens for $\lambda\sim 7.6$.

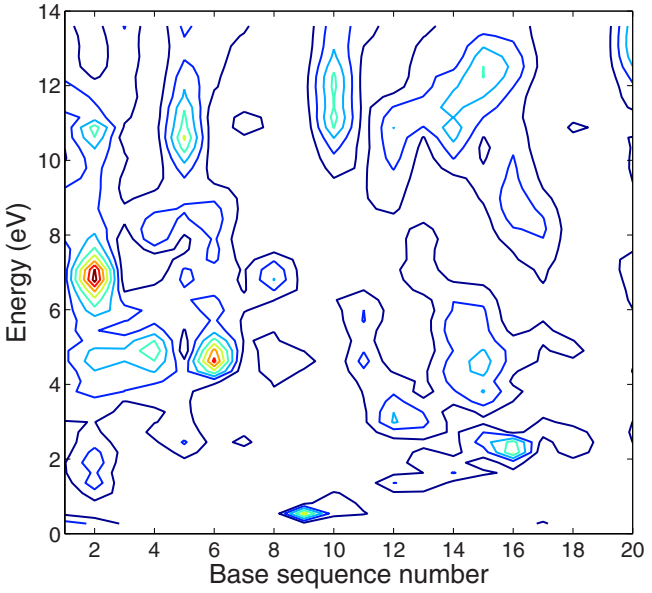

FIG. 4. (Color online) Contour plot of the square of the wave function at each base's center for the poly(A)·poly(T) decamer as a function of energy and base sequence number n. Contour lines are equally spaced at integer values.

We can now also answer the question of whether there is appreciable enhancement of the partial capture factors at low energy. Figure 3(b) clearly says so for energies less than say 3 eV, a region of interest for the low-energy $l=2,3$ shape resonances of the bases [32] (see Fig. 6, showing cross sections of the four bases).

B. B-form GCGAATTGGC base pairs decamer

Now that we know how to look for internal diffraction, let us repeat the analysis of the preceding section on our sequence disordered decamer for $\vec{k}$ perpendicular to the mid-

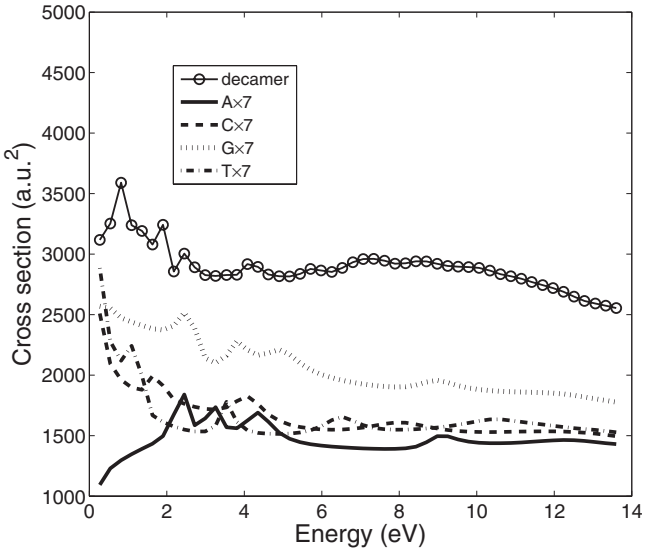

FIG. 6. Interpolated total elastic cross section as a function of incident electron energy for the GCGAATTGGC B-form decamer compared with the single adenine, cytosine, guanine, and thymine *R*-matrix cross-section values.

section base-pair direction and the spiral axis.

The total elastic cross section as a function of energy using the full extent of angular momenta $l \leqslant 8$ exhibits a cross section that has peaks some 500 times the geometrical one. This confirms the unphysical behavior of this procedure at low energy. Using the interpolation procedure, however, restores a credible cross section as shown in Fig. 6. A comparison with the cross section of individual bases again reveals a satisfactory correspondence of most peak structures. Figure 7 shows the quantity $\Gamma_w(0)$, equal to the average of the square of the electron wave function on the bases. It is

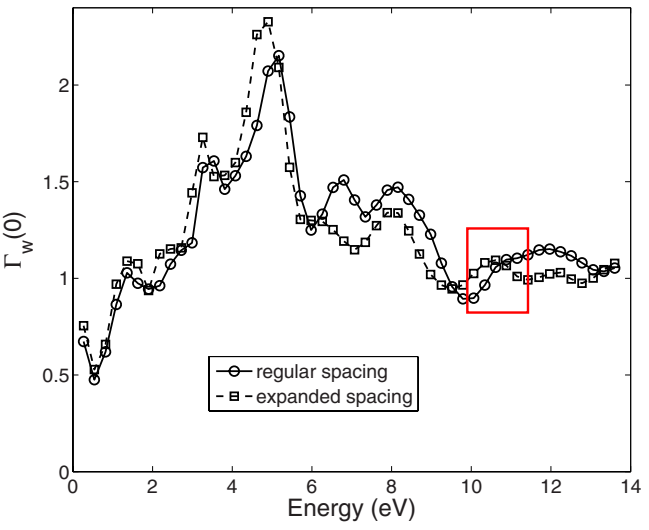

FIG. 7. (Color online) Interpolated value of the average of the square of the electron wave function on the bases as a function of incident electron energy for the GCGAATTGGC B-form decamer for normal spacing and with an expanded spacing 1.05 times the regular one. The rectangular area highlights the peak structure at 11.4 eV discussed in the text.

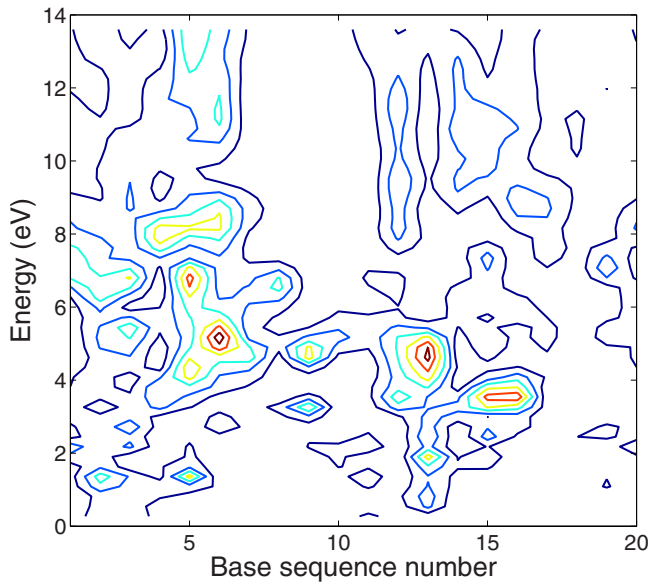

FIG. 8. (Color online) Contour plot of the square of the wave function at each base's center for the GCGAATTGGC B-form decamer as a function of energy and base sequence number *n*. Contour lines are equally spaced at integer values.

compared to the one obtained by dilating the distances along the spiral axis by a factor 1.05. The diffraction signature around 11.4 eV is still present but with an appreciably reduced enhancement factor relative to the plane-wave value of 1. This is the effect of sequence disorder, which turns out to be stronger than what was anticipated from the toy model calculations. The lower-energy structures are similar to those of the poly(A)·poly(T) decamer. Figure 8 shows a contour plot of $\gamma(0,\vec{R}_n)$, the absolute square of the wave function at each base's center, in energy and base sequence space. The sequencing index varies from 1 to 10 going up the GCGAATTGGC strand and from 11 to 20 going down the complementary strand. The peak structures in $\Gamma_w(0)$ of Fig. 7 showing appreciable enhancement of the wave function are seen to occur mostly in the midregion, on the base pairs that lie mostly perpendicular to the incident electron direction. Sequence disorder has a visible effect on the interference patterns within the decamer and not only on internal diffraction. It somewhat desynchronizes the ends from the midsection. The somewhat irregular distribution of the peaks at lower energies ($E \lesssim 8$ eV) in both decamers studied thus far shows that these structures are local ones and perhaps a signature of weak localization. Localization has been predicted in poly(dA)·poly(dT) decamer studies due to structural changes promoted by thermal fluctuations [26]. There is a parallel to be made between the time evolution of localized states and our energy dependence. The axially scattered current in the $+\hat{z}$ direction (from the G end to the C end) shown in Fig. 9(a) also presents a clear diffraction peak. But the large peak at 9.2 eV in Fig. 5(a) has now disappeared, stressing the importance of sequence disorder. The forward scattered current of Fig. 9(b) shows no evidence of internal diffraction. This parameter is less sensitive to internal diffraction, as was already evident from the poly(A)·poly(T) results. The weighted partial capture factors are very similar to the poly(A)·poly(T) one.

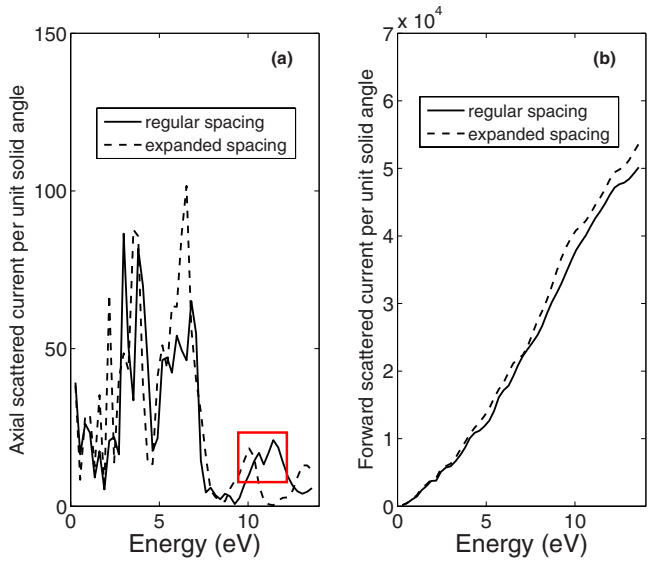

FIG. 9. (Color online) Scattered current in a.u. for the B-form GCGAATTGGC decamer as a function of incident electron energy for normal spacing and for an expanded spacing 1.05 times the regular one: (a) in the $+\hat{z}$ direction; (b) in the forward direction.

C. A-form GCGAATTGGC base pairs decamer

We finally look at the A-form of the GCGAATTGGC base pairs decamer. Its geometry being sufficiently different from the B-form justifies looking for variances in the scattering results.

Figure 10 shows the cross section for this A-form decamer. One immediately notices the globally smaller values by some 10–15 % compared to its B-form analog in Fig. 6. This was unexpected in view of the closer packing of the base pairs and of the results from the toy model [29], which led us to expect larger capture factors due to MS. This emphasizes the need for realistic scattering models. This might well be a geometric effect due to the 30% larger rise of the B-form. In order to explore this hypothesis, we have stretched the A-form by increasing the rise and helical twist to agree with the B-form values, but keeping the base pair tilt and roll intact. Figure 10 shows the cross section for this stretched decamer. One recovers the same scale of values as for the B-form decamer. So although the geometrical cross section of the stretched A-form is 30% larger, the cross section is only 10–15 % larger. It would seem that there is an additional effect counterbalancing this certainly caused by changing MS interference as the base pairs get farther away from one another. Note that there is no internal diffraction to be seen in the A-form in the chosen energy range. The distance between nearest base pairs (the rise) is too small, which pushes the diffraction effects to energies beyond 13.6 eV.

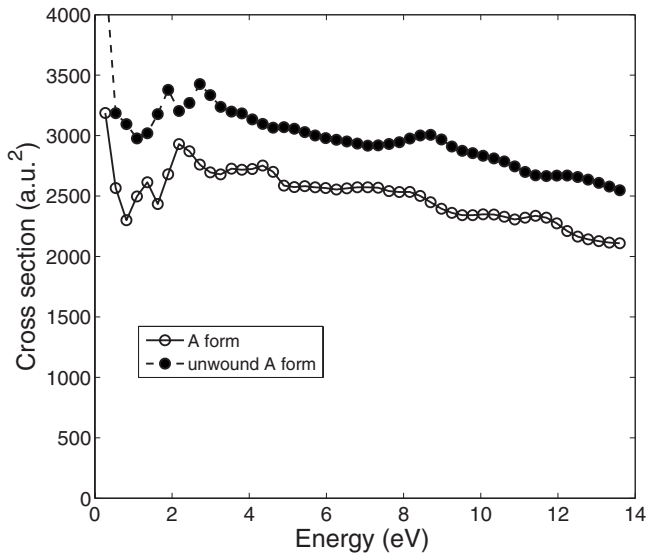

FIG. 10. Interpolated total elastic cross section of the GCGAATTGGC A-form decamer (open circles) and of the stretched counterpart having B-form rise and helical twist (black circles) as a function of incident electron energy.

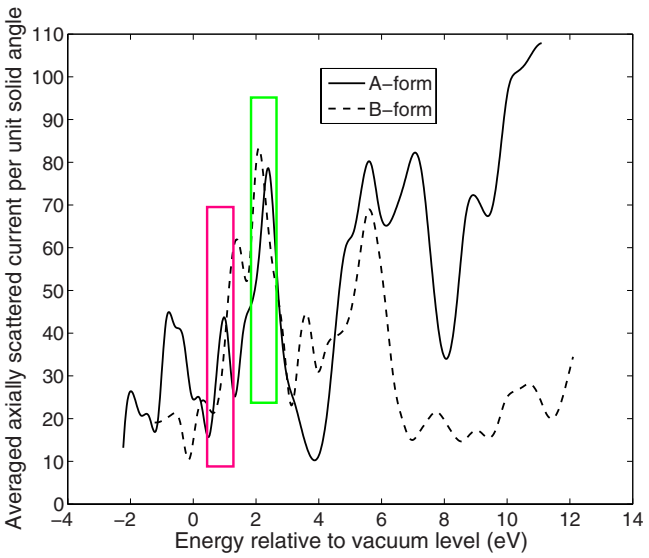

FIG. 11. (Color online) Average of the scattered current in a.u. in the two axial directions and for two incident and mutually orthogonal directions of the GCGAATTGGC A-form and B-form decamers as a function of incident electron energy. The two rectangular areas highlight the regions around 0.8 and 2.2 eV discussed in the text.

Finally, we have computed scattering parameters for both the A and B forms, which are more easily comparable with existing experimental data. The averaged electron current scattered along the DNA axis ($\pm Z$ scattered directions and X, Y incident directions) is shown in Fig. 11 as a function of electron energy. Similarly, the magnitude of the square of the wave function averaged over all bases is shown in Fig. 12. In both figures, the data have been interpolated using cubic spline to produce smoother-looking curves. To facilitate comparison with experimental data, the zero electron energy is shifted by the estimated value U_{op} of the polarization energy. This shift is necessary, since in thin-film experiments with electrons incoming from vacuum, the zero energy is conveniently referenced to that of the vacuum level. The U_{op} values for the A and B forms were evaluated by estimating the polarization energy on a base due to its near neighbors. As we wish to make comparisons with experimental results

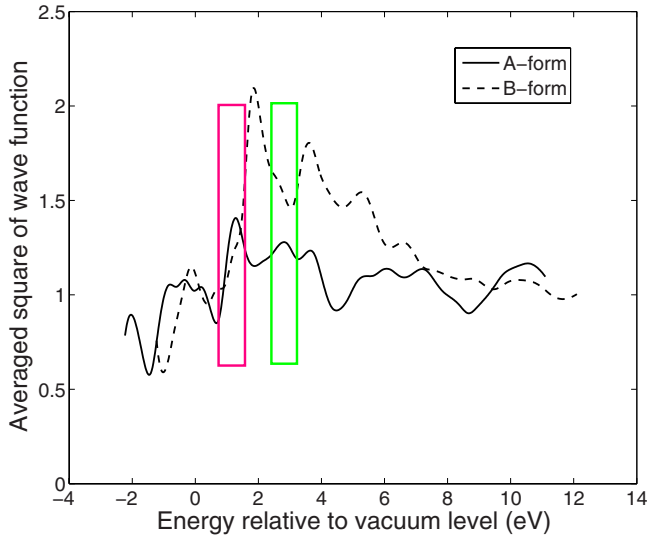

FIG. 12. (Color online) Average of the square of the electron wave function on the bases over two incident and mutually orthogonal directions of the GCGAATTGGC A-form and B-form decamers as a function of incident electron energy. The two rectangular areas highlight the regions around 1.3 and 2.8 eV discussed in the text.

on DNA, we have added an interaction with the nearest phosphate and deoxyribose subunits as well as to some four [64] close structural water molecules that would be present in real DNA. We have utilized the formula $U_{\mathrm{op}} \approx -\Sigma\alpha/(2d^4)$, where α was given an average value of 100 (a.u.)^3 for the in-plane polarizability of the partner base [65] an average value of 47 (a.u.)^3 for the out-of-plane polarizability of the two axial neighbors [65], an average value of 5 and 80 (a.u.)^3 for the isotropic polarizabilities of phosphate and deoxyribose, respectively [66], and of 10 (a.u.)^3 for the water molecules [67]. We used a distance $d \sim 11$ a.u. for the partner distance and 7 a.u. for all other distances [64] except for the A-form axial nearest-neighbor distance, which was taken to be 5.3 a.u. Needless to say, the values obtained for U_{op}, −1.5 and −2.5 eV for the B-form and A-form, respectively, are approximate although credible. Typical widths for the interference peaks are two to three times the calculation resolution of 0.272 eV. This is compatible with a number of experiments (see [15] for instance).

IV. COMPARISON BETWEEN THEORY AND EXPERIMENTS

Low-energy electron (LEE) experiments with DNA have been performed on dry films, in ultrahigh vacuum, where the molecule adopts the A-form owing to nonstructural water loss [68]. These experiments have measured the damage inflicted to DNA mostly by electrons in the 0–20 eV range, i.e., the yield functions, in the form of base [8,69], sugar [70] and phosphate lesions [71], single and double strand breaks [1,72,73], and base release [74]. Thus, no electron scattering experiments are presently available to be directly compared to our theoretical results. However, some of the mechanisms, which have been invoked to account for the magnitude of the yield of specific damages and peak energies in their yield functions below 15 eV, rely on scattering properties of LEE within the DNA molecule.

In experiments with thin films of plasmid DNA, the yield function for single strand breaks (ssb) exhibits maxima at 0.8, 2.2, and 10 eV, with a shoulder at 6 eV [1,15,72], which appears as a distinctive peak at this energy in the ssb yield function of synthetic single-stranded DNA films [75]. The peak positions were determined with an accuracy of 0.3 eV. From the analysis of LEE-induced products from this latter type of films, the yield function for base release was also found to exhibit peaks at 6 and 10 eV [75]. Below 15 eV, the yield function for the induction of double strand breaks (dsb) was found to be dominated by a single peak located at 10 eV [1,73]. Owing to their low energies, the 0.8 and 2.2 eV maxima could easily be interpreted as shape resonances [15], but the exact mechanism leading to rupture of the C-O phosphodiester bond (i.e., ssb) [74] is not obvious for two reasons. First, the cross section for ssb induction below 3 eV is of the order of 10^{-17} cm^2 per base pair [76], which is fairly large for damage caused by a single anion dissociative state at 0.8 and 2.2 eV, respectively. In fact, this value is almost as large as that measured at 100 eV, in the same DNA, where a plethora of ionization and dissociation channels are available [73,76]. Interference enhancement of the electron wave function within DNA may therefore increase at low energies the electron capture cross section of transient anion states responsible for ssb. Secondly, in the experiment of Martin *et al.* [15], the 0.8 and 2.2 eV peaks did not coincide with the energy of the dissociative phosphate anion, which is known to rupture the C-O bond of the DNA backbone [74]. Instead, these peaks coincided with those in the electron capture cross section of the DNA bases. The latter result led Martin *et al.* [15] to postulate that the electron was first captured by the basis and then transferred to the phosphate group.

In fact, according to the theoretical studies of Simons' group, below 3 eV electrons cleave the CO bond of the DNA backbone at the 3′ and 5′ positions essentially via electron transfer. [6,77–79] An electron is first captured by a base to form a π^* transient anion and afterward the additional electron transfers, via the sugar moiety, to the phosphate unit where it occupies a σ^* orbital at either the 3′ or 5′ C-O positions. The resulting anion state being dissociative leads to C-O bond cleavage (i.e., a ssb). Electron transfer is not necessarily limited to the nucleotide where capture occurs [80,81]. Thus, if the main mechanism leading to ssb is electron transfer from the bases, the large cross section for damage below 3 eV could be explained by invoking strong constructive interference of the electron wave function due to stacking of the bases along the DNA chain.

This cross section could maximize at 0.8 and 2.2 eV, if the incoming electron preferably scatters along the DNA axis at these energies, where it would cause preferential interference enhancement due to base stacking. This is quite compatible with what is found in the energy dependence of the magnitude of the electron current scattered along the axis of A-DNA in Fig. 11: the current in the Z direction is maximized near 0.8 and 2.2 eV. When DNA is modified to its B form, the two peaks move closer to each other and little correlation is found with the experimental values. In Fig. 12, the average of the square of the scattered electron wave func-

tion on a base is found to maximize near 1.3 and 2.8 eV, in fair agreement with the experimental maxima in the yield function for ssb. Thus, by including both the shape resonance wave functions and constructive interference due to base stacking, our calculation can represent fairly well the energy dependence of the yield of ssb below 3 eV.

A comment here is warranted on the precision of the match between experimental and theoretical results. There are two main sources of uncertainty in the position of the calculated peaks: the resonances calculated by R matrix are shifted too high by roughly 1 eV, and the potential U_{op} by which we shift the graphs in Figs. 11 and 12 is also approximate. But the influence of the energy of the shape resonances on the position of the peaks in the figures is uncertain as these are probably mostly MS interference effects. In this case, the resonances have only a mild modulation effect on the cross section. Therefore, we believe that the peak features of Figs. 11 and 12 might be shifted by some 1 eV or less, mostly due to the uncertainty in U_{op}, thus not coinciding perfectly with the experimental features. With such a large uncertainty in the theoretical peak energies, good correlation can also be found between the calculated peaks for the B form in Fig. 12 and those of the experiments. Nevertheless, the combined A-DNA form data from Figs. 11 and 12 appear to be a better match to the experimental data. In any case, since dry DNA is in the A form, any correlation between the theoretical peaks of the B form and experimental ones must be considered somewhat fortuitous.

The broad 6-eV feature in the experimental ssb yield function of DNA, which spreads from 5 to 7 eV [75], is also in good agreement with the theoretical results of Figs. 11 and 12 for the A-form. Both curves exhibit two peaks around 6 eV, which if unresolved would produce a broad maximum around 6 eV, as observed experimentally.

The 6-eV feature has been studied in detail by Zheng *et al.*, who bombarded thin molecular films of a short single strand of DNA, with electrons of energies between 4 and 15 eV [75]. By high-pressure liquid chromatography, they identified 12 fragments of the oligonucleotide GCAT sequentially composed of the bases guanine (G), cytosine (C), adenine (A), and thymine (T). The yield functions exhibited maxima at 6 and 10–12 eV, which were interpreted as due to the formation of transient anions leading to fragmentation. Later, they analyzed the products induced by 4–15 eV electrons incident on two abasic forms of the tetramer GCAT, i.e., XCAT and GCXT, where X represents the base, which has been removed and replaced by a hydrogen atom [82]. The results obtained at an incident energy of 6 eV showed that essentially no strand break occurs at positions in the backbone corresponding to those of the missing base. *This finding clearly indicated that at* 6 eV, *and possibly below, electrons break the DNA backbone almost exclusively via electron transfer*. Furthermore, the total yield of all the bases released and ssb induced by electrons were found to be strongly affected by the presence of an abasic site; in both XCAT and GCXT, the yield of detached bases was found to be up to an order of magnitude smaller than that from GCAT [82]. Thus, the initial electron capture amplitude was suggested to be highly sensitive to the number and possibly the geometrical arrangement of the bases, indicating the presence of a strong collective effect. According to the results of Figs. 11 and 12, this collective effect could be related to strong electron scattering on axis around 6 eV, which exhibits an eightfold increase in magnitude in going from 4 to 6 eV. Interference enhancement of the scattered electron wave function around 6 eV could also play an important role. Both phenomena should be highly sensitive to base removal, since they are directly related to base stacking and their periodicity.

Finally, the maximum near 10 eV in the electron energy dependence of the calculated averaged axial scattered current and the square of the wave function averaged on all bases for the A-form correlate well with the strong maximum found experimentally in the yield function for ssb and dsb induced by LEE impact on plasmid DNA [1,73]. This result suggests that coherence also influences DNA damage in the 10 eV region, i.e., at energies where the formation of core excited resonances is the dominant mechanism implicated in bond rupture [2]. Such anion states, which consist of two electrons occupying electronically excited orbitals around a positive hole of a DNA subunit, are highly localized [2]. It is not obvious how such anion states would couple to a diffracted wave along the DNA axis, a problem that has not been addressed in the present work. Furthermore, present and previous [29,30] partial wave analysis of the enhanced electron capture probability on specific subunits due to diffraction has been show to be much reduced in the 10 eV region compared to low energies. It is therefore possible that the energy coincidence mentioned above is fortuitous.

To check the validity of all of our comparisons, we calculated the averaged electron current scattered along the DNA axis (Z direction) and the magnitude of the square of the wave function averaged over all bases for different base sequences of the A-form. We observe a fairly good stability in the features of the curves up to about 7 eV. In other words, the effect of diffraction is not very dependent on sequence and therefore a comparison with experimental data obtained with different sequences can be considered significant below 7 eV. Thus, the stability of the structural information in Figs. 11 and 12 with different base sequences and the comparison with experimental results indicate that wave-function interference should be taken into account to describe the mechanism of action of electrons with energies lower than 7 eV in DNA. Beyond this value, the energy of the calculated minima and maxima changes according to sequence. Thus in this case, multiple scattering of the electron wave in DNA is highly sequence-dependent, and comparison with data obtained with plasmid DNA, which is longer and has a different sequence, is not considered to be significant.

V. CONCLUSIONS

This paper describes an attempt to use high-quality gas phase scattering data to gain insight into the interaction, in condensed phase, of DNA and low-energy electrons, which is relevant for radiation damage to nucleic acids by ionizing radiation. In particular, we used R-matrix calculations performed by some of us [16] for the gas phase scattering. To explore the interaction of a continuum electron with the

DNA double strand, we couple the gas phase calculations with a multiple scattering framework developed by some of us [28–31] a few years ago. The combination of *R*-matrix calculations and multiple scattering has been recently shown [58,59] to give accurate results for simpler systems such as the water dimer and ice. These recent works have also inspired the angular momentum cutoff procedure and the interpolation of the scalar quantities described in Sec. III.

The results we show here, in a similar fashion to Refs. [28–31], show that some peaks in electron scattering from macromolecules can be due to diffraction instead of formation of negative anions. They also show that single basis calculations are not enough to gain an understanding of the process and that collective effects can be as important as local ones.

Despite the simplicity of our model, we found fairly good correlation between calculated values for the A-form and experimental results obtained on LEE-induced damage to DNA in this configuration. Below 7 eV, the calculated averaged electron current scattered along the DNA axis (*Z* direction) and the magnitude of the square of the electron wave function, averaged over all bases for different base sequences of the A-form, were found to be essentially independent of the nature and sequence of the bases. It was therefore possible to compare calculated values with the results of experiments performed with a longer DNA molecule of a different sequence. The structures that appeared in the calculated current scattered along the DNA axis and the square of the wave function correlated well with the maxima found in the yield function for breaking a single and two adjacent strands of DNA by the impact of 0–7 eV electrons. The correlation indicates that a substantial increase in DNA damage occurs at the energies of preferential scattering of the incoming electron along the DNA axis, i.e., at energies where interference enhancement occurs due to base stacking. Although our results for A-DNA and B-DNA are not markedly different, theory-experiment correlation appears to be better for the A-form, which is likely to be the one present in thin-film experiments [29]. It appears from both comparisons that diffraction effects within DNA should be taken into account to describe the mechanism of action of electrons with energies below 7 eV. This may also hold true for higher energies, but it is difficult to compare the present calculations with experimental data beyond 7 eV, because core-excited resonances implicated in the damaging process were not included in our model and because the energy dependence of the scattered current and of the square of the wave function change according to sequence.

Our model constitutes an attempt to relate the gas phase and condensed phase areas of the research in electron scattering from biomolecules. The model is far from perfect since it has many assumptions. In particular, it is difficult to draw solid conclusions on radiation damage from this model, first of all because we consider only elastic scattering events, and completely neglect the motion of the nuclei, which would add a prohibitive new level of complexity. Also, considering DNA as rigid is far too simplistic in solution but also to some extent in thin films where at best the material can be considered "amorphous" and structural water is present anyway. The motion of the electron in the liquid should also be considered, and it would be best to use an electron distribution taken from photoemission in a biological medium like water instead of using a plane wave [83]. One simple improvement to the model could be to consider structural water, with positions taken possibly from relevant DNA crystal structures, and we are planning to explore this possibility to gain a better understanding of the role of disorder and parasite scatterers.

ACKNOWLEDGMENTS

S.T. is supported by NSF and NSEC. The work of C.H.G. has been supported partly by an allocation of NERSC supercomputing resources that were used to perform the *R*-matrix calculations, and in part by the U.S. Department of Energy, Office of Science. L. S. was supported by the Canadian Institutes of Health Research.

[1] B. Boudaïffa, P. Cloutier, D. Hunting, M. A. Huels, and L. Sanche, Science **287**, 1658 (2000).
[2] For a review, see L. Sanche, Eur. Phys. J. D **35**, 367 (2005).
[3] V. Cobut, Y. Frongillo, J. Patau, T. Goulet, M.-J. Fraser, and J.-P. Jay-Gerin, Radiat. Phys. Chem. **51**, 229 (1998).
[4] S. Pimblott and J. A. LaVerne, Radiat. Phys. Chem. **76**, 1244 (2007).
[5] A. Bass and L. Sanche, Radiat. Environ. Biophys. **37**, 243 (1998), a review paper.
[6] R. Barrios, P. Skurski, and J. Simons, J. Phys. Chem. B **106**, 7991 (2002).
[7] A. M. Scheer, K. Aflatooni, G. A. Gallup, and P. D. Burrow, Phys. Rev. Lett. **92**, 068102 (2004).
[8] X. Pan, P. Cloutier, D. Hunting, and L. Sanche, Phys. Rev. Lett. **90**, 208102 (2003).
[9] A. Migus, Y. Gauduel, J. L. Martin, and A. Antonetti, Phys. Rev. Lett. **58**, 1559 (1987).
[10] C. V. Sonntag, Adv. Quantum Chem. **52**, 5 (2007).
[11] U. Uehara, H. Nikjoo, and D. Goodhead, Radiat. Res. **152**, 202 (1999).
[12] S. Denifl, S. Ptasińska, M. Probst, J. Hrušák, P. Scheier, and T. Märk, J. Phys. Chem. A **108**, 6562 (2004); see citations therein.
[13] S. Ptasinska, S. Denifl, S. Gohlke, P. Scheier, E. Illenberger, and T. D. Mark, Angew. Chem., Int. Ed. **45**, 1893 (2006).
[14] K. Aflatooni, G. A. Gallup, and P. D. Burrow, J. Phys. Chem. **102**, 6205 (1998).
[15] F. Martin, P. D. Burrow, Z. Cai, P. Cloutier, D. Hunting, and L. Sanche, Phys. Rev. Lett. **93**, 068101 (2004).
[16] S. Tonzani and C. H. Greene, J. Chem. Phys. **122**, 014111 (2005).
[17] D. Bouchiha, J. D. Gorfinkiel, L. G. Caron, and L. Sanche, J. Phys. B **39**, 975 (2006).
[18] A. Grandi, F. A. Gianturco, and N. Sanna, Phys. Rev. Lett. **93**, 048103 (2004).
[19] C. S. Trevisan, A. E. Orel, and T. N. Rescigno, J. Phys. B **39**, L255 (2006).
[20] C. Winstead and V. McKoy, Phys. Rev. A **73**, 012711 (2006).

[21] J. Gu, Y. Xie, and H. F. Schaefer III, J. Am. Chem. Soc. **127**, 1053 (2005).
[22] S. Kim, S. E. Wheeler, and H. F. Schaefer III, J. Chem. Phys. **124**, 204310 (2006).
[23] C. F. Craig, W. R. Duncan, and O. V. Prezhdo, Phys. Rev. Lett. **95**, 163001 (2005).
[24] N. T. Maitra, J. Chem. Phys. **125**, 014110 (2006).
[25] A. Wasserman, N. T. Maitra, and K. Burke, J. Chem. Phys. **122**, 144103 (2005).
[26] J. P. Lewis, T. E. Cheatham III, E. B. Starikov, H. Wang, and O. F. Sankey, J. Phys. Chem. B **107**, 2581 (2003).
[27] F. D. Lewis, L. Zhang, X. Liu, X. Zuo, D. M. Tiede, H. Long, and G. C. Schatz, J. Am. Chem. Soc. **127**, 14445 (2005).
[28] L. G. Caron and L. Sanche, Phys. Rev. Lett. **91**, 113201 (2003).
[29] L. Caron and L. Sanche, Phys. Rev. A **70**, 032719 (2004).
[30] L. Caron and L. Sanche, Phys. Rev. A **72**, 032726 (2005).
[31] L. Caron and L. Sanche, Phys. Rev. A **73**, 062707 (2006).
[32] S. Tonzani and C. H. Greene, J. Chem. Phys. **124**, 054312 (2006).
[33] T. M. Orlando, D. Oh, Y. Chen, and A. B. Aleksandrov, J. Chem. Phys. **128**, 195102 (2008).
[34] D. Chandler and K. Leung, Annu. Rev. Phys. Chem. **45**, 557 (1994).
[35] This sequence was extracted from the ideal 36 base pairs theoretical models of DNA in the atlas of macromolecules of the Protein Explorer at http://www.umass.edu/microbio/chime/pe_beta/pe/atlas/atlas.htm.
[36] M. Feig and B. M. Pettitt, Biophys. J. **75**, 134 (1998).
[37] S. Neidle, *Nucleic Acid Structure and Recognition* (Oxford University Press, New York, 2002).
[38] D. Dill and J. L. Dehmer, J. Chem. Phys. **61**, 692 (1974).
[39] J. B. Pendry, *Low Energy Electron Diffraction* (Academic, London, 1974).
[40] G. A. Fiete and E. J. Heller, Rev. Mod. Phys. **75**, 933 (2003).
[41] N. F. Mott and H. S. W. Massey, *The Theory of Atomic Collisions* (Clarendon, Oxford, 1965), 3rd ed.
[42] F. A. Gianturco and A. Jain, Phys. Rep. **143**, 347 (1986).
[43] A. Messiah, *Quantum Mechanics* (Wiley, New York, 1962), Appendix C.
[44] T. F. O'Malley and H. S. Taylor, Phys. Rev. **176**, 207 (1968).
[45] M. A. Morrison and L. A. Collins, Phys. Rev. A **17**, 918 (1978).
[46] C. Froese-Fischer, T. Brage, and P. Jonsson, *Computational Atomic Structure* (Insitute of Physics, Bristol, 1997).
[47] S. Tonzani, Comput. Phys. Commun. **176**, 146 (2007).
[48] S. Tonzani and C. H. Greene, J. Chem. Phys. **125**, 094504 (2006).
[49] M. Aymar, C. H. Greene, and E. Luc-Koenig, Rev. Mod. Phys. **68**, 1015 (1996).
[50] Bioengineering Institute, The University of Auckland, New Zealand, *Fem/bem notes* (1997), http://www.bioeng.auckland.ac.nz/cmiss/fembemnotes/fembemnotes.pdf.
[51] Scientific Computing Group, University of Basel, *Pardiso*, http://www.computational.unibas.ch/cs/scicomp/software/pardiso/.
[52] S. Hara, J. Phys. Soc. Jpn. **27**, 1009 (1969).
[53] R. G. Parr and W. Yang, *Density Functional Theory of Atoms and Molecules* (Oxford University Press, Oxford, 1989).
[54] C. Lee, W. Yang, and R. G. Parr, Phys. Rev. B **37**, 785 (1988).
[55] R. R. Lucchese, F. A. Gianturco, and N. Sanna, Chem. Phys. Lett. **305**, 413 (1999).
[56] F. A. Gianturco and J. A. Rodriguez-Ruiz, Phys. Rev. A **47**, 1075 (1993).
[57] S. Tonzani, Ph.D. thesis, JILA and Department of Chemistry, University of Colorado, Boulder (2001).
[58] L. Caron, D. Bouchiha, J. D. Gorfinkiel, and L. Sanche, Phys. Rev. A **76**, 032716 (2007).
[59] D. Bouchiha, L. G. Caron, J. D. Gorfinkiel, and L. Sanche, J. Phys. B **41**, 045204 (2008).
[60] B. Segall and F. S. Ham, in *Energy Bands of Solids*, edited by B. Alder, S. Fernbach, and M. Rotenberg, Vol. 8 of *Methods in Computational Physics* (Academic, New York, 1968), p. 251.
[61] G. C. Fletcher, *The Electron Band Theory of Solids* (North-Holland, Amsterdam, 1971).
[62] D. A. Case, Annu. Rev. Phys. Chem. **33**, 151 (1982).
[63] C. R. Natoli, D. K. Misemer, S. Doniach, and F. W. Kutzler, Phys. Rev. A **22**, 1104 (1980).
[64] A working hypothesis based on the examination of x-ray data of DNA found in the Nucleic Acid Database at http://ndbserver.rutgers.edu/ and the Protein Data Base at http://www.pdb.org/pdb/home/home.do.
[65] H. Basch, D. R. Garmer, P. G. Jasien, M. Krauss, and W. J. Stevens, Chem. Phys. Lett. **163**, 514 (1989).
[66] Values obtained from the ACD/ChemSketch Freeware, version 10.00, Advanced Chemistry Development, Inc., Toronto, ON, Canada, www.acdlabs.com, 2006.
[67] T. N. Olney, N. M. Cann, G. Cooper, and C. E. Brion, Chem. Phys. **223**, 59 (1997).
[68] S. Swarts, M. Sevilla, D. Becker, C. Tokar, and K. Wheeler, Radiat. Res. **129**, 333 (1992).
[69] H. Abdoul-Carime and L. Sanche, Int. J. Radiat. Biol. **78**, 89 (2002).
[70] Z. Cai, M.-E. Dextraze, P. Cloutier, D. Hunting, and L. Sanche, J. Chem. Phys. **124**, 024705 (2006).
[71] X. Pan and L. Sanche, Phys. Rev. Lett. **94**, 198104 (2005).
[72] L. Sanche, Radiat. Prot. Dosim. **99**, 57 (2002).
[73] M. A. Huels, B. Boudaïfa, P. Cloutier, D. Hunting, and L. Sanche, J. Am. Chem. Soc. **125**, 4467 (2003).
[74] Y. Zheng, P. Cloutier, D. Hunting, R. Wagner, and L. Sanche, J. Am. Chem. Soc. **127**, 16592 (2005).
[75] Y. Zheng, P. Cloutier, D. J. Hunting, J. R. Wagner, and L. Sanche, J. Chem. Phys. **124**, 064710 (2006).
[76] R. Panajotovic, F. Martin, P. Cloutier, D. J. Hunting, and L. Sanche, Radiat. Res. **165**, 452 (2006).
[77] J. Berdys, I. Anusiewicz, P. Skurki, and J. Simons, J. Am. Chem. Soc. **126**, 6441 (2004).
[78] J. Berdys, P. Skurski, and J. Simons, J. Phys. Chem. B **108**, 5800 (2004).
[79] J. Berdys, I. Anusiewicz, P. Skurski, and J. Simons, J. Phys. Chem. A **108**, 2999 (2004).
[80] H.-A. Wagenknecht, Nat. Prod. Rep. **23**, 973 (2006).
[81] B. Giese, J. Amaudrut, A.-K. Köhler, M. Spormann, and S. Wessely, Nature **412**, 318 (2006).
[82] Y. Zheng, J. R. Wagner, and L. Sanche, Phys. Rev. Lett. **96**, 208101 (2006).
[83] M. Allan, J. Electron Spectrosc. Relat. Phenom. **48**, 219 (1989).